



Cite this: DOI: 10.1039/c5dt02941d

## Solutions of complex copper salts in low-transition-temperature mixture (LTTM)†

Maxim A. Zakharov,<sup>a</sup> Gennady V. Fetisov,<sup>a</sup> Alexei A. Veligzhanin,<sup>b</sup> Michael A. Bykov,<sup>a</sup> Ksenia A. Paseshnikchenko,<sup>a</sup> Sergei F. Dunaev<sup>a</sup> and Leonid A. Aslanov<sup>\*a</sup>

The structure and properties of diethanolamine complexes of copper(II) triflates dissolved in an excess of diethanolamine (DH<sub>2</sub>) were studied. The copper containing substance was found to be a solution of copper(II) complex salt [Cu<sup>2+</sup>DH<sub>2</sub>(DH<sup>-</sup>)]OTf<sup>-</sup> in LTTM composition [(DH<sub>2</sub>)<sub>4</sub>H<sup>+</sup>](OTf<sup>-</sup>), where LTTM = low-transition-temperature mixture, OTf<sup>-</sup> = triflate anion. According to the EXAFS data, the coordination number of copper(II) atoms in solution does not exceed four. Addition of even negligible amounts of acid significantly changes DH<sub>2</sub> volatility and decomposition conditions.

Received 30th July 2015,  
Accepted 29th September 2015  
DOI: 10.1039/c5dt02941d

www.rsc.org/dalton

## Introduction

Ionic liquids (ILs) are intensively studied due to the variety and specificity of their properties opening wide perspectives of their application. Beginning from 2003,<sup>1</sup> deep eutectic solvents (DES)<sup>2–5</sup> have also been used. DES are more convenient than ILs: they are cheaper and easier to produce, and their properties are very close to those of ILs. Later a special group of solvents, low-transition-temperature mixtures (LTTMs),<sup>6</sup> was introduced. These solvents have no eutectic point and hence differ from DES.

Recently, a new group of ionic liquids, MetILs<sup>7–10</sup> (ionic liquids with metal coordination cation) with transition metal ions as coordination centers and amino alcohols as ligands, were suggested. MetILs are very attractive for application in molecular magnets,<sup>11–14</sup> galvanoplastics<sup>15–17</sup> and for production of novel electric accumulators.<sup>18</sup> They have two advantages: low price and high metal concentration which cannot be obtained in solutions of salts.<sup>19,20</sup>

Earlier it was shown<sup>21</sup> that diethanolamine (DH<sub>2</sub>) and copper ions form complexes [CuDH<sub>2</sub>]<sup>2+</sup> at pH 6.0–6.4, but at pH 7.2–11.0 the OH groups are deprotonated, and [CuDH<sub>2</sub>DH]<sup>+</sup> cations or neutral [Cu(DH)<sub>2</sub>] complexes are formed with increasing pH.

Tauler and co-workers<sup>22</sup> found that in the pH range 3–12 only mononuclear complexes with chelating diethanolamine ligands are formed in aqueous solutions. However, binuclear

Cu(II) complexes were obtained and their crystal structures solved.<sup>23,24</sup> In these complexes, the deprotonated hydroxyl groups form bridges between copper atoms. The earlier data on Cu(II) complex formation with diethanolamine are summarized in a review.<sup>25</sup>

There are a lot of interesting findings<sup>7–10</sup> related to the synthesis, structure and properties of MetILs with general formula MA<sub>2</sub>·6L, where M = Fe(III), Cu(II), Mn(II), Zn(II); A = CF<sub>3</sub>SO<sub>3</sub><sup>-</sup> = OTf (triflate anion), N(SO<sub>2</sub>CF<sub>3</sub>)<sub>2</sub><sup>-</sup> = NTF<sub>2</sub> (bis(trifluoromethylsulfonyl)imide), CH<sub>3</sub>(CH<sub>2</sub>)CH(C<sub>2</sub>H<sub>5</sub>)COO<sup>-</sup> = EHN (2-ethylhexanoate ion); L = DH<sub>2</sub> or EH (ethanolamine). All the obtained MetILs are considered to be individual coordination compounds rather than solutions of transition metal salts or their complexes in the presence of an excess of ligand.<sup>7–10</sup> In all MetILs the coordination number of the metal atom is six.

Crystals of [CuDH<sub>2</sub>DH]OTf were isolated from MetILs of composition Cu(OTf)(EHN)·6DH<sub>2</sub>. The crystal structure was solved and it appeared that:<sup>9</sup> (1) only two DH<sub>2</sub> of six are in the inner coordination sphere of Cu atom; (2) both DH<sub>2</sub> are chelating ligands forming coordination bonds *via* the N and O atoms; (3) one of the hydroxyl groups bound to Cu atom is deprotonated. It should be noted that deprotonation of the hydroxyl groups in the presence of amines usually yields metal alcoholates;<sup>27,28</sup> ethanolamine forms alcoholates under the same conditions as alcohols<sup>29</sup> and can form alcoholates even without addition of secondary and tertiary amines, yielding the ammonium tautomer.<sup>30</sup> And last (4), but not least: the Cu(II) coordination number is 4 + 2, which is typical of Cu(II) cations. Based on the above mentioned crystal structure, a hypothesis that Cu(OTf)(EHN)·6DH<sub>2</sub> and Cu(OTf)<sub>2</sub>·6DH<sub>2</sub> can be solutions of a Cu(II) complex salt in DES or LTTM must not be excluded. This hypothesis is tested in the present work.

The only problem not considered in ref. 7–10 is the localization of the hydroxyl group proton split out due to complex

<sup>a</sup>Department of Chemistry, Lomonosov Moscow State University, Moscow, 119991, Russian Federation. E-mail: aslanov@struct.chem.msu.ru; http://www.chem.msu.su/; Tel: +7 495 9391327

<sup>b</sup>NRC Kurchatov Institute, Kurchatov Square 1, Moscow, 123182, Russian Federation  
† Electronic supplementary information (ESI) available. See DOI: 10.1039/c5dt02941d

formation. A concept of “proton wires” or “proton pumps” has been widely developed in modern biology. This concept mainly considers migration of protons *via* chains of water molecules with formation of oxonium ions, although special attention is also paid to ammonium cations and hydrogen bonds formed between them and N-heterocycles or amino groups.<sup>31–34</sup> A model of proton transport *via* a chain of ammonia molecules<sup>35</sup> considers a block  $\text{H}_3\text{N}\cdots\text{H}^+\cdots\text{NH}_3$  as the central unit. This block has been found in the crystalline state<sup>36</sup> and is analogous to the well-studied stable ion  $\text{H}_5\text{O}_2^+$  in which a proton is coordinated by two oxygen atoms.<sup>26</sup> Crystal structures of more complex aggregates of ammonium cations and ammonia molecules with short and strong hydrogen bonds are also known.<sup>37</sup> The enthalpy of reaction (1) in the gaseous phase is  $\sim 17 \text{ kcal mol}^{-1}$  for  $n = 0$ , slightly lower than  $17 \text{ kcal mol}^{-1}$  for  $n = 1$  and  $\sim 15 \text{ kcal mol}^{-1}$  for  $n = 2$ .<sup>38</sup>



According to ref. 26, a proton can bind to the O atoms of hydroxyl groups in the presence of super-acids. Under such conditions,<sup>39</sup> protons form a dynamical system composed of O–H  $\sigma$ -bonds and O $\cdots$ H hydrogen bonds, in which the  $\sigma$ -bonds and hydrogen bonds can interchange places; this is equal to a rapid migration of charge of the super-acid proton between all the ligands. A similar dynamical system is supposed to exist for super-acidic proton addition to primary and secondary amines, because the electron affinity of ammonia and amines is higher than that of water, alcohols and ethers.<sup>40</sup> Volatility of ligands is decreased in the presence of onium salts, and this is one of the key properties of  $\text{Cu}(\text{OTf})_2 \cdot 6\text{DH}_2$  and DES.

The structures of metal complexes in crystals and liquids can be different, that is why we have studied coordination numbers of metal atoms in  $\text{Cu}(\text{OTf})_2 \cdot 6\text{DH}_2$  compared with some other compounds (see Table 1) by EXAFS and also investigated the properties of the  $\text{DH}_2$ -HOTf system.

## Experimental section

### Materials and reagents

Reagents used in the present research  $\text{HN}[(\text{CH}_2)_2\text{OH}]_2$  (99%, Acros),  $\text{H}_2\text{N}(\text{CH}_2)_6\text{OH}$  (97%, Aldrich),  $\text{H}_2\text{N}(\text{CH}_2)_2\text{OH}$  (99%, Sigma-Aldrich),  $\text{Cu}_2(\text{OH})_2\text{CO}_3$  (95%, Aldrich),  $\text{Fe}(\text{NO}_3)_3 \cdot 9\text{H}_2\text{O}$  (98%, Sigma-Aldrich),  $\text{FeCl}_3 \cdot 6\text{H}_2\text{O}$  (97%, Sigma-Aldrich),  $\text{CF}_3\text{SO}_3\text{H}$  (99%, Acros) were taken without further purification.

**Table 1** The list of investigated samples

Designation	Chemical composition
$\text{Cu}(\text{OTf})_2 \cdot 6\text{EH}$	$\text{Cu}(\text{CF}_3\text{SO}_3)_2 \cdot 6\text{H}_2\text{N}(\text{CH}_2)_2\text{OH}$
$\text{Cu}(\text{OTf})_2 \cdot 6\text{HH}$	$\text{Cu}(\text{CF}_3\text{SO}_3)_2 \cdot 6\text{H}_2\text{N}(\text{CH}_2)_6\text{OH}$
$\text{Fe}(\text{OTf})_3 \cdot 6\text{HH}$	$\text{Fe}(\text{CF}_3\text{SO}_3)_3 \cdot 6\text{H}_2\text{N}(\text{CH}_2)_6\text{OH}$
$\text{Fe}(\text{OTf})_3 \cdot 6\text{DH}_2$	$\text{Fe}(\text{CF}_3\text{SO}_3)_3 \cdot 6\text{HN}[(\text{CH}_2)_2\text{OH}]_2$
$\text{Cu}(\text{OTf})_2 \cdot 6\text{DH}_2$	$\text{Cu}(\text{CF}_3\text{SO}_3)_2 \cdot 6\text{HN}[(\text{CH}_2)_2\text{OH}]_2$

### Synthesis

The samples investigated in this research are listed in Table 1 with their designations and chemical formulae. These compositions were synthesized in two stages. In the first stage,  $\text{Cu}(\text{II})$  triflate<sup>41</sup> and  $\text{Fe}(\text{III})$  triflate<sup>42</sup> were prepared by the known methods.

In the second stage, the final compositions were obtained by mixing the corresponding metal triflate and amino alcohol. Full details are given in the ESI.†

### Analytical methods

**Differential thermal analysis-thermogravimetry-mass spectrometry (DTA-TG-MS).** Simultaneous thermogravimetry and analysis of the decomposition products by mass spectrometry were performed using a Netzsch STA-409 PC/PG analyzer, heating rate of  $5 \text{ }^\circ\text{C min}^{-1}$ , argon stream  $40 \text{ l min}^{-1}$ .

**Differential scanning calorimetry (DSC).** Samples were analyzed using a Netzsch DSC-204 F1 analyzer in a high purity nitrogen flow  $40 \text{ ml min}^{-1}$  with the standard aluminum cells, temperature range  $130\text{--}60 \text{ }^\circ\text{C}$ , heating and cooling rates  $5 \text{ }^\circ\text{C min}^{-1}$  with temperature detection error  $0.1^\circ$ .

**Infrared spectroscopy.** The FTIR spectra in the wavenumber range of  $500\text{--}4000 \text{ cm}^{-1}$  were recorded using the Perkin-Elmer SPECTRUM ONE FTIR spectrometer.

**MALDI mass spectrometry.** MALDI mass spectra were recorded using a Bruker Autoflex II MALDI-TOF MS. The spectrometer (FWHM resolution 18 000) had a nitrogen laser with wavelength 337 nm and a time of flight mass analyzer operating in the reflection mode. Samples were applied on a polished stainless steel substrate. The spectrum was recorded in the positive ion mode. The resulting spectrum was the sum of 300 spectra obtained at different points of a specimen. Anthracene (Acros, 99%) served as a matrix.

### EXAFS spectroscopy for local structure analysis

Local structure of liquids was studied by EXAFS spectroscopy within the energy range about the X-ray absorption K-edge of the metal atoms in the investigated substances. The modern theoretical and practical basics of this method can be found, for example, in a book by Fetisov<sup>43</sup> (chapter 5). More detailed description of structural analysis by XAFS methods including the detailed instruction is given by G. Bunker in the Manual Guide.<sup>44</sup>

The X-ray absorption spectra around K-edges of the metals present in the investigated liquids have been recorded in the transmission mode on the X-ray beam line “The Structural Materials Science”<sup>45</sup> (bending magnet source, “Siberia-2” storage ring at Kurchatov Synchrotron Radiation Source (KSRS), Moscow, Russia) equipped with a Si(111) channel-cut monochromator having energy resolution  $\Delta E/E \sim 2 \times 10^{-4}$ . The ring was operated at 2.5 GeV with the electron currents decaying from 45 to 35 mA. The size of the SR beam at the sample location was  $1 \text{ mm (V)} \times 2 \text{ mm (H)}$ . EXAFS spectra were recorded in transmission mode using ionization chambers filled with air. The ionization current of the chambers was measured with Keithley 6487 picoamperemeters. We used

three ionization chambers: two of them measured the intensity of the primary ( $I_0$ ) and transmitted intensity through the sample ( $I_t$ ) radiation beams. The sample was located between these ionization chambers on the path of the primary beam. The third chamber measured the intensity ( $I_s$ ) of the SR beam passing through the reference sample which was used for absolute calibration of photon energy. The foil made of the metal in the investigated liquid served as the reference.

The absorption spectra of the samples were recorded step-by-step within the energy interval from  $-170$  to  $+800$  eV relative to the K-edge of absorbing metal atoms. The reference elements in our EXAFS experiments were Fe and Cu having K-edges of 7112.0 and 8979.0 eV, respectively.

In order to optimize the measurement procedure, the specified data collection interval was divided into three segments: the pre-edge region (from  $-170$  to  $-20$  eV), the near-edge segment ( $-20$ – $80$  eV), and EXAFS oscillation area ( $80$ – $800$  eV). In the first segment the data were measured with steps of 10 eV, the step was  $\sim 0.5$  eV in the near-edge region, and the last segment was scanned with an equidistant step of  $0.05 \text{ \AA}^{-1}$  on a scale of  $k$  – photoelectron momentum. The measurement exposure time  $T$  in EXAFS area increased depending on point number  $n$  quadratically as ( $T = an^2 + c$ ), to compensate for the decrease in the EXAFS oscillation amplitude with increasing energy. The constants  $a$  and  $c$  of this expression were chosen so that the initial exposure for 2 s at the end of the segment was increased to 8 s. Thus, each spectrum was measured for *ca.* 30 min.

**Samples investigated by EXAFS.** The list of samples studied by EXAFS is presented in Table 1. Studies on  $\text{Fe}(\text{OTf})_3 \cdot 6\text{HH}$  and  $\text{Fe}(\text{OTf})_3 \cdot 6\text{DH}_2$  are auxiliary and these results are presented in ESI.† The samples of liquids for EXAFS measurements were prepared in two ways. In the first case, a drop of liquid was deposited on an ashless paper filter. This filter was folded in several layers (2–6) to get the absorption jump value  $\Delta(\mu d)$  close to unity. In the second case, a self-sustaining film was formed due to surface tension in the hole made in a substrate foil (aluminum). The magnitude  $\Delta(\mu d)$  of the absorption jump in this case was controlled by selecting the thickness of foil. Due to low vapor pressure of IL, DES or LTTM, drying and noticeable change in the film thickness of the sample during the measurement period was not observed.

**EXAFS data analysis.** Processing of EXAFS data was performed using the IFEFFIT<sup>46,47</sup> package, version 1.2.11c. The data were first processed by the ATHENA program of this package to fit and subtract their complex background, to normalize the absorption spectrum by unity jump and then to separate the oscillating part of the spectrum – the X-ray absorption fine structure (XAFS). The fine structure extracted in such a way was used for further structural analysis.

The parameters of the local structure of liquid around the resonantly absorbing (reference) atom were determined and refined by fitting the theoretical EXAFS spectrum calculated for a selected hypothetical model of the structure to the experimental one. This refinement was carried out by the ARTEMIS program, version 0.08.014 from the IFEFFIT package and

conducted in direct space  $R$ , using the phase and amplitude of electron scattering calculated with aid of the FEFF 8.20.19 program.

Depending on the spectrum complexity, calculations were carried out either in approximation of one coordination sphere and single scattering of electrons, or by using two or three coordination spheres.

Such a modeling allows refinement of distance from the absorbing atom to the nearest neighbors  $R_j$ ; the root-mean-square deviation in bond distances between atom pairs  $\sigma_j^2$  accounting for thermal vibration and statistical local disorder;<sup>48</sup> the central atom coordination numbers  $N_j$  relative to the nearest neighbors. The threshold energy  $E_0$  of the photoelectron impulses relative to the K absorption edge was also refined. The amplitude reduction factor  $S_0^2$  present in the main EXAFS equation was set to 0.8 so that to exclude its correlation effect on the defined coordination numbers.

## Results and discussion

### Results of structural analysis by EXAFS.

**Choice of the  $S_0^2$  coefficient value.** The value and oscillation mode of EXAFS signal are dependent on the scattering of photoelectrons ejected at the X-quantum absorption and on the types of atoms surrounding the resonantly absorbing central metal atom, that is, the local structure of the studied sample. However, along with photoelectron energy loss at the cost of scattering on atoms of the coordination environment, additional energy loss on excitation of all the system of electrons of the studied sample (multielectron excitation) is also possible. At present a complete theory accounting for this effect is absent, that is why an empirical coefficient  $S_0^2$ , also denoted as a passive electron decrease in EXAFS signal has been included to the main EXAFS equation by Rehr and Albers.<sup>49</sup> This coefficient serves for quantitative fitting of the theoretically calculated EXAFS amplitudes to experimental ones. The role and physical sense of the  $S_0^2$  coefficient has been widely discussed.<sup>48–53</sup>

Choice of the value of  $S_0^2$  coefficient is very important for structural analysis using EXAFS. The “proper”  $S_0^2$  value was considered in detail by Campbell *et al.*<sup>51</sup> It was concluded that the effect of multielectron excitations caused by a photoelectron in the course of EXAFS is negligible, the most probable  $S_0^2$  value is 0.9 with possible deviations of several percent. It was also calculated that the  $S_0^2$  value depends only slightly on the electron’s energy and scattering pathway, that is, it is almost equal for all the pathways of electron scattering and all EXAFS spectra. J. Rehr, one of elaborators of analysis of EXAFS spectra, considers<sup>48–53</sup> that in the absence of adequate theory describing the  $S_0^2$  coefficient, it should be approximated by a constant of  $0.9 \pm 0.1$  (see also <http://millennia.cars.aps.anl.gov/pipermail/ifeffit/2002-October/000155.html>).

Due to a correlation coefficient between  $S_0^2$  and coordination numbers  $N_j$  in the EXAFS equation being almost equal to unity, it is impossible to determine the  $N_j$  value properly

if the  $S_0^2$  value is unknown. It should be noted that the amplitude reduction coefficient value practically does not have any effect on statistical characteristics of fitting and the radii of coordination spheres (Table 2,  $R_f$  and  $R$ ) but significantly changes  $N_j$  values.

In order to justify the choice of  $S_0^2$  value, we used its refinement in an EXAFS IL model with known and fixed coordination numbers, namely, Fe1 IL sample – 1-butyl-3-methylimidazolium tetrachloroferrate(III) ( $C_4H_9NC_3H_3NCH_3$ ) [ $FeCl_4$ ]. The EXAFS spectrum of this IL is well approximated by a simple model of single scattering with one coordination sphere consisting of exactly four Cl atoms. The refinement data for the basic sample at various fixed  $S_0^2$  values are given in Table 2. As can be seen, coordination number  $N = 4$  for Fe atoms is attained at  $S_0^2 \sim 0.8$  and at the higher  $N$  values  $S_0^2$  appears to be significantly underestimated.<sup>54</sup>

Refinement of the model at the fixed  $N = 4$  gave  $S_0^2 = 0.8 \pm 0.08$ . That is why for other studied samples we used  $S_0^2 = 0.8$  in model refinement and  $N_j$  determination.

**EXAFS of  $Cu(CF_3SO_3)_2 \cdot 6HN(CH_2)_2OH$ , and  $Cu(CF_3SO_3)_2 \cdot 6H_2N(CH_2)_6OH$ .** These studies helped to understand formation of complexes of copper atoms in solutions of amino alcohols. As the local structure model for  $Cu(OTf)_2 \cdot 6EH$  and  $Cu(OTf)_2 \cdot 6HH$  samples was complicated beginning from the one sphere model, the best correspondence with the experimental EXAFS data characterized by statistical  $R_f$  criterion was attained using three coordination spheres containing N and C atoms as shown in Table 3. Supposing  $S_0^2 = 0.8$  and a model with three coordination spheres, the coordination number of amino groups around Cu atom is between 3.0 and 4.0 for both samples, but somewhat larger for  $Cu(OTf)_2 \cdot 6EH$  sample; in this case coordination mode with two chelate metalocycles consisting of five atoms and providing coordination number of four can be expected. In the case of  $Cu(OTf)_2 \cdot 6HH$  sample, chelation is less probable due to the ligand length, and amino alcohol molecules seem to be monodentate ligands with N-donating atoms, because affinity of Cu atoms to the amino groups is higher than to the hydroxyl groups.

According to Table 3, the coordination number of copper atoms in  $Cu(OTf)_2 \cdot 6EH$  and  $Cu(OTf)_2 \cdot 6HH$  samples does not exceed four, but co-existence of complexes with three- and four-coordinated copper atoms cannot be ruled out.

**EXAFS of  $Cu(CF_3SO_3)_2 \cdot 6HN(CH_2)_2OH$ .** Metalocycles were found in the crystal structure of  $[Cu\{NH(CH_2CH_2OH)_2\}\{NH(CH_2CH_2OH)(CH_2CH_2O)\}CF_3SO_3]CF_3SO_3 = [CuDH_2DH]OTf$ .<sup>9</sup> The coordination polyhedron of Cu atom in these crystals was tetragonal bipyramidal with coordination number of 4 + 2, typical of copper complexes.

However, our results indicate that coordination number of Cu atom in liquid preparation  $Cu(OTf)_2 \cdot 6DEA$  is not more

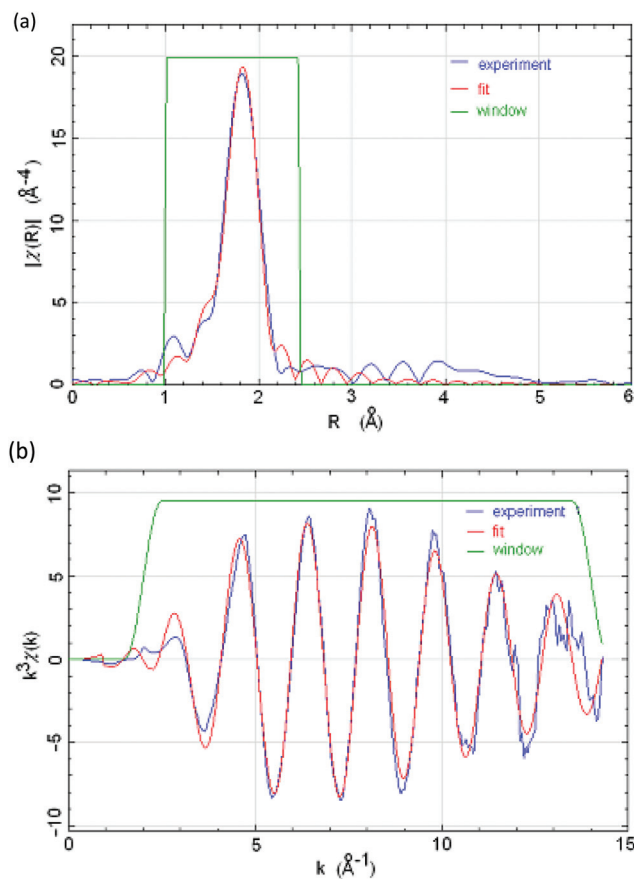


**Fig. 1** Fitting of EXAFS spectrum of Fe1 IL ( $C_4H_9NC_3H_3NCH_3$ )[ $FeCl_4$ ] by a single-sphere model with  $N = 4$  and single photoelectron scattering via Fe–Cl pathway in (a) metrical  $R$  and (b) wave  $k$  spaces. Weighting functions are depicted in green,  $S_0^2$  being  $0.8 \pm 0.08$ .

**Table 2** EXAFS model parameters vs. the amplitude reduction factor  $S_0^2$  for a sample ( $C_4H_9NC_3H_3NCH_3$ )[ $FeCl_4$ ] Fe1 with known coordination number of chlorine atoms ( $N_{Fe}$ ) in the metal atom environment<sup>a</sup>

Sample	$S_0^2$	$E_0/eV$	Scattering path	$N_{Fe}$	$R/\text{Å}$	$10^3 \sigma^2/\text{Å}^2$	$R_f$ (%)
Fe1	<b>1.0</b>	$3.1 \pm 1.2$	Fe–Cl	$3.2 \pm 0.31$	$2.204 \pm 0.005$	$3.3 \pm 0.6$	1.75
Fe1	<b>0.9</b>	$3.1 \pm 1.2$	Fe–Cl	$3.5 \pm 0.34$	$2.204 \pm 0.005$	$3.3 \pm 0.6$	1.75
Fe1	<b>0.8</b>	$3.1 \pm 1.2$	Fe–Cl	$4.0 \pm 0.4$	$2.204 \pm 0.005$	$3.3 \pm 0.6$	1.75
Fe1	$0.8 \pm 0.08$	$3.1 \pm 1.2$	Fe–Cl	<b>4.0</b>	$2.204 \pm 0.005$	$3.3 \pm 0.6$	1.75

<sup>a</sup> Calculations were performed using rectangle window weighting functions (Fig. 1) of width 2.000–14.000  $\text{Å}^{-1}$  and 1.000–2.450  $\text{Å}$  in the impulse  $k$  space and direct  $R$  space, respectively. Parameters fixed at fitting are given in bold type. The EXAFS spectrum of the basic sample was obtained at the same station by the same method and treated by the same procedure as the spectra of all samples studied in this work. The best-fitting  $S_0^2$  coefficient obtained for this basic sample (Fe1) was used as an approximation of the amplitude reduction factor for all the studied samples.

**Table 3** The local structure parameters of samples with Cu cation<sup>a</sup>

Sample, model	Scattering pathway	$N_j$	$R/\text{\AA}$	$10^3\sigma^2/\text{\AA}^2$	$R_f$ (%)
Cu(OTf) <sub>2</sub> ·6EH, 3 spheres	Cu-(N/O)	3.6 ± 0.34	2.014 ± 0.006	4.8 ± 0.8	2.0
	Cu-C1	1.35 ± 0.6	2.78 ± 0.03		
	Cu-C2	1.46 ± 0.7	2.97 ± 0.04		
Cu(OTf) <sub>2</sub> ·6HH, 3 spheres	Cu-(N/O)	3.3 ± 0.3	2.025 ± 0.007	4.8 ± 0.8	2.17
	Cu-C1	1.3 ± 0.6	2.98 ± 0.04		
	Cu-C2	0.9 ± 0.5	2.73 ± 0.04		

<sup>a</sup> Calculations were performed at approximation of the amplitude reduction factor by  $S_0^2$  constant = 0.8 with the rectangle window weighting functions (Fig. 1) 2.000–14.000  $\text{\AA}^{-1}$  and 1.0–3.0  $\text{\AA}$  in width in impulse  $k$  and direct  $R$  spaces, respectively. For nitrogen and carbon atoms in the considered coordination spheres,  $\sigma^2$  factors are supposed to be equal.

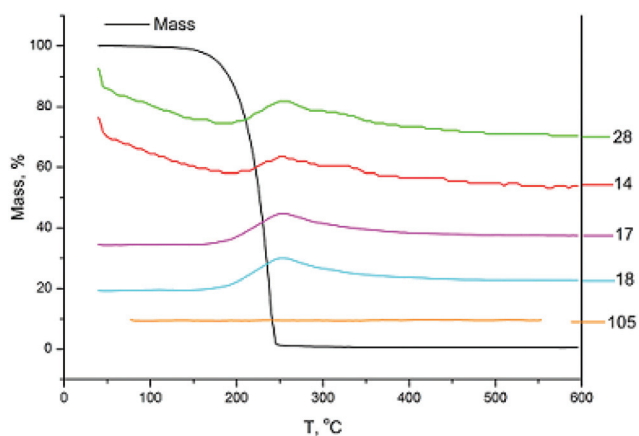
**Table 4** The local structure parameters of samples containing DH<sub>2</sub> ligand. Calculations performed for  $S_0^2 = 0.8$ , fitting in the range  $k = 2\text{--}12 \text{\AA}^{-1}$ ,  $R = 1.2\text{--}3.2 \text{\AA}$ 

Sample	$S_0^2$	Scattering pathway	$N_j$	$R/\text{\AA}$	$10^3\sigma^2/\text{\AA}^2$	$R_f$ (%)
Cu(OTf) <sub>2</sub> ·6DH <sub>2</sub>	0.8	Cu-(N/O)	3.0 ± 0.6	1.99 ± 0.01	1.1 ± 1.5	5.1
		Cu-C	2.2 ± 1.8	2.84 ± 0.03	2.0 ± 7.0	

than four (Table 4). Taking into account the above mentioned data, hereafter we shall use a formula  $[\text{Cu}^{2+}\text{DH}_2(\text{DH}^-)]\text{--}[(\text{DH}_2)_4\text{H}^+](\text{OTf}^-)_2$  instead of  $\text{Cu}(\text{OTf})_2\cdot 6\text{DH}_2$ .

### Volatility of DEA and its mixtures

DH<sub>2</sub> as an individual compound was subjected to thermogravimetry with the simultaneous measurement of the mass spectra of exit vapors and gases. Many DH<sub>2</sub> fragments including water vapor are evolved in the range 200–250 °C (Fig. 2), indicating not only DH<sub>2</sub> decomposition but possibly its condensation reaction. The latter reaction can yield a number of products including dimers *N,N,N*-tris(hydroxyethyl)ethylenediamine and *N,N*-bis(hydroxyethyl)piperazine, which were detected by heating DH<sub>2</sub> to 250 °C.<sup>55</sup>

**Fig. 2** TGA curve of pure DH<sub>2</sub> and the simultaneously recorded mass spectra of exit vapors and gases.

Mass spectra indicate that DH<sub>2</sub> does not vaporize (Fig. 2). Thus, various reactions proceed in the course of TGA, and this means that this method of study is flawed for the studied system and its results should not be used for conclusions about non-volatility of DH<sub>2</sub> in MetILs.

DH<sub>2</sub> was unambiguously detected when  $[\text{Cu}^{2+}\text{DH}_2(\text{DH}^-)]\text{--}[(\text{DH}_2)_4\text{H}^+](\text{OTf}^-)_2$  was studied by MALDI spectrometry (ESI, Fig. S3†); this possibly came from laser knocking of DEA molecules without heating the substance.

To study the proton effect on the properties of  $[\text{Cu}^{2+}\text{DH}_2(\text{DH}^-)]\text{--}[(\text{DH}_2)_4\text{H}^+](\text{OTf}^-)_2$ , we prepared and studied additional preparations, the first of them being  $[\text{DH}_3^+]\text{OTf}^-$ . Amino alcohols form crystalline ammonium salts with strong acids. DSC curves presented in Fig. 3a indicate that  $[\text{DH}_3^+]\text{OTf}^-$  is a typical ionic liquid.

For comparison, the DSC curve of DH<sub>2</sub> is presented in Fig. S4 (ESI†). Both DSC curves (Fig. S4† and 3a) do not exclude possible formation of a eutectic in a pseudo-binary system  $[\text{DH}_3^+]\text{OTf}^-$ –DH<sub>2</sub> (DES formation).

Usually DES consist of ammonium salts and H-bond acceptors in molar ratio 1 : 2, that is why we prepared the second additional preparation,  $[(\text{DH}_2)_3\text{H}^+]\text{OTf}^-$ , to check the possible formation of a eutectic.

DSC heating and cooling curves of this preparation are presented in Fig. 4b and c, respectively. In the absence of an exothermic extremum of cold crystallization, the endothermic extremum on heating curve of the cooled preparation can be interpreted as transfer from the glassy state of the mixture to a plastic state, which is typical of amorphous systems. We failed to detect a eutectic and thus can not assign the  $[\text{DH}_3^+]\text{OTf}^-$ –DH<sub>2</sub> system to DES.

The studied system differs in acidic residues from the most existing DES. Chloride ions surrounded by an envelope of H-bond donor molecules are typically used in DES, whereas in

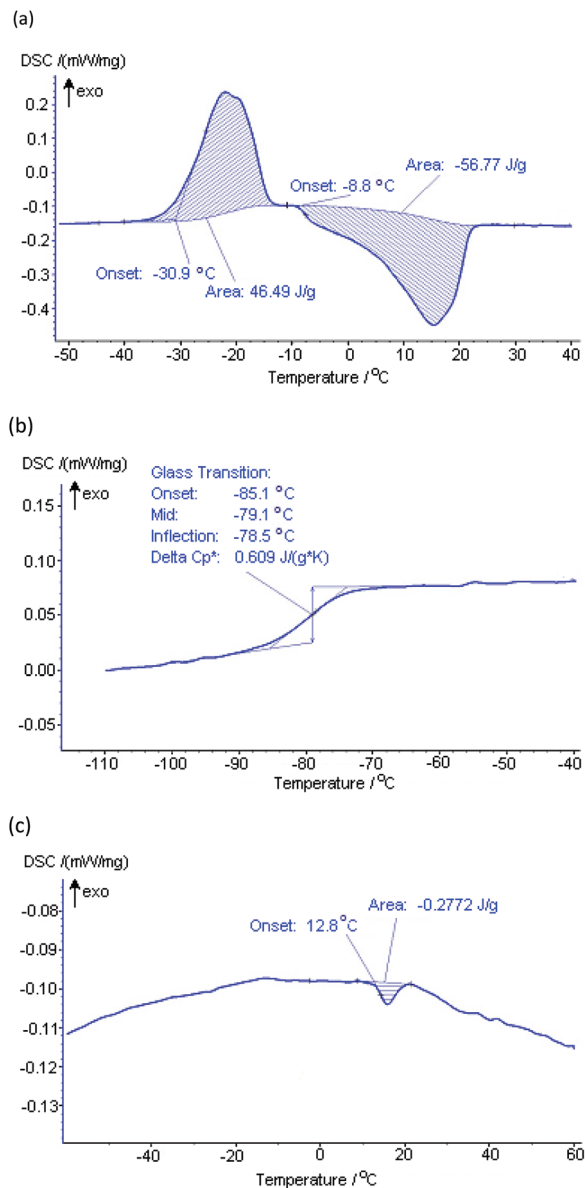


Fig. 3 DSC curves of additional preparations: (a)  $[\text{DH}_3^+]\text{OTf}^-$  heating; (b)  $[(\text{DH}_2)_3\text{H}^+]\text{OTf}^-$  cooling; (c)  $[(\text{DH}_2)_3\text{H}^+]\text{OTf}^-$  heating.

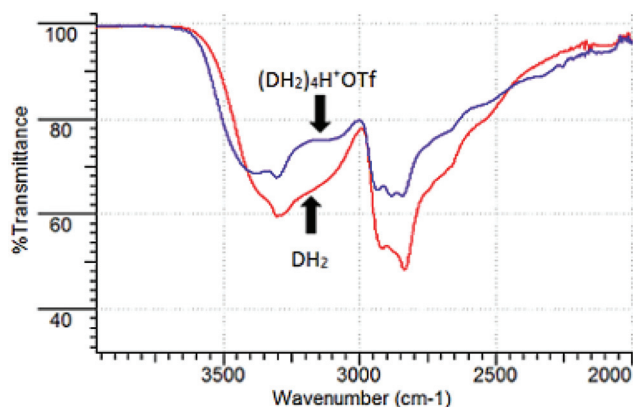


Fig. 4 IR spectrum of  $(\text{DH}_2)_4\text{H}^+\text{OTf}^-$  compared with that of  $\text{DH}_2$ .

$[\text{DH}_3^+]\text{OTf}^-$ - $\text{DH}_2$  system the acidic residue belongs to a super-acid and thus is a very weak base, which hardly forms hydrogen bonds and does not need to be in an isolating envelope because of a weak interaction with a proton. In the  $[\text{DH}_2^+]\text{OTf}^-$ - $\text{DH}_2$  system, protons can localize on the N or O atoms of  $\text{DH}_2$  molecules, but N atoms are preferential, because the proton affinity of N atoms in amine molecules is higher than that of O atoms in alcohol molecules.<sup>40</sup>

Accounting for the aforesaid,  $[(\text{DH}_2)_3\text{H}^+]\text{OTf}^-$  should be assigned to low-transition-temperature mixtures<sup>6</sup> (LTTMs) rather than to DES. We studied a third additional preparation,  $[(\text{DH}_2)_4\text{H}^+]\text{OTf}^-$ , because  $[\text{Cu}^{2+}\text{DH}_2(\text{DH}^-)][(\text{DH}_2)_4\text{H}^+](\text{OTf}^-)_2$  can be regarded as a solution of a crystalline phase  $[\text{Cu}^{2+}\text{DH}_2(\text{DH}^-)]\text{OTf}^-$  in liquid phase  $[(\text{DH}_2)_4\text{H}^+]\text{OTf}^-$ .

The IR spectrum of the latter preparation shown in Fig. 4 surprisingly coincides with the IR spectrum of  $\text{Cu}(\text{OTf})_2 \cdot 6\text{DEA}^2$  (see Fig. 2b).

In the absence of copper atoms in  $(\text{DH}_2)_4\text{H}^+\text{OTf}^-$ , shifts of the IR bands should be rationalized by protonation of the amine and hydroxyl groups of DEA.

Thermogravimetric study of this preparation combined with mass spectrometry showed that DEA does not vaporize, but in contrast to  $\text{DH}_2$ ,  $(\text{DH}_2)_4\text{H}^+\text{OTf}^-$  decomposes in two stages (Fig. 5 and S5 of ESI<sup>†</sup>): about 280 °C only water vapor is evolved; this fact indicates that  $\text{DH}_2$  molecules condense without decomposition, and various  $\text{DH}_2$  fragments are evolved at 410 °C.

So, protonation of  $\text{DH}_2$  amine and possibly hydroxyl groups results in a noticeable change in the pathway of  $\text{DH}_2$  condensation and decomposition in  $(\text{DH}_2)_4\text{H}^+\text{OTf}^-$  as compared with pure  $\text{DH}_2$  (possibly due to acidic catalysis). A decomposition temperature 410 °C at atmospheric pressure corresponds to the decomposition temperature of many ILs including  $\text{DH}_3^+\text{OTf}^-$ . Mass loss of  $(\text{DH}_2)_4\text{H}^+\text{OTf}^-$  at heating to 360 °C (Fig. 5) corresponds with a loss of three  $\text{DH}_2$  mole fractions out of four.

The  $\text{DH}_2$  condensation products seem to vaporize without decomposition, because they contain less atom groups able to form H-bonds. This can compensate for vaporization tempera-

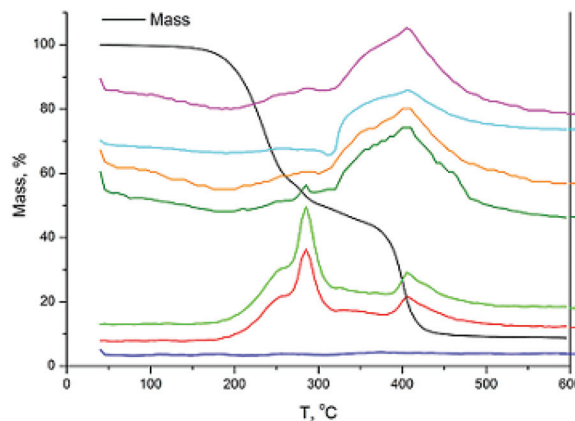


Fig. 5 TGA curve of  $(\text{DH}_2)_4\text{H}^+\text{OTf}^-$  and the simultaneously recorded mass spectra of exit vapors and gases.

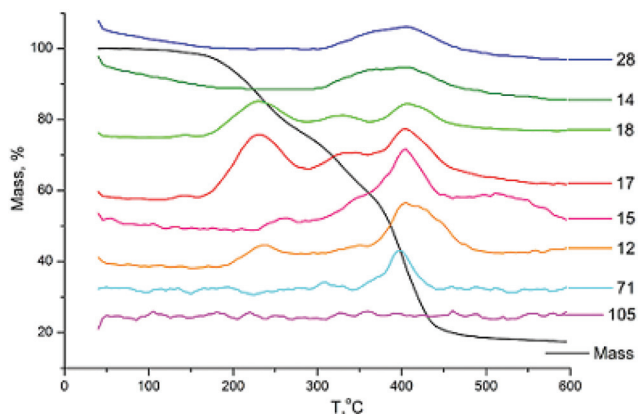


Fig. 6 TGA curve of  $[\text{Cu}^{2+}\text{DH}_2(\text{DH}^-)][(\text{DH}_2)_4\text{H}^+](\text{OTf}^-)_2$  and the simultaneously recorded mass spectra of exit vapors and gases.

ture increase inevitable on molecular mass increase and that is why  $\text{DH}_2$  condensation products can vaporize without decomposition, in contrast to  $\text{DH}_2$ .

$[\text{Cu}^{2+}\text{DH}_2(\text{DH}^-)][(\text{DH}_2)_4\text{H}^+](\text{OTf}^-)_2$  was subjected to TGA and mass spectrometry (Fig. 6). As can be seen, there are three waves of  $\text{DH}_2$  decomposition product release, corresponding to water vapor, in the absence of  $\text{DH}_2$  vaporization. Three waves of decomposition possibly indicate the existence of three different kinds of  $\text{DH}_2$  molecules in  $[\text{Cu}^{2+}\text{DH}_2(\text{DH}^-)][(\text{DH}_2)_4\text{H}^+](\text{OTf}^-)_2$ : those coordinated to  $\text{Cu}^{2+}$  ions, as well as protonated and non-bound molecules.

Analogous to Fig. 5, the first wave water vapor (not decomposition products) release at  $\sim 230$  °C, can be assigned to condensation of protonated  $\text{DH}_2$  molecules. The second wave of water vapor release (320 °C) can be considered as a result of condensation of  $\text{DH}_2$  molecules coordinated to  $\text{Cu}(\text{II})$  ions, because no water vapor was detected in other preparations at 320 °C. Condensation reaction at this temperature can be catalyzed by  $\text{Cu}(\text{II})$  ions.<sup>56</sup> Both condensation waves are not accompanied by release of products of  $\text{DH}_2$  thermolysis. Finally, a distinct third wave (410 °C) of decomposition products release corresponds with thermolysis of IL  $[\text{DH}_3^+]\text{OTf}^-$  marked in Fig. 5.

Comparing the properties of DES and LTTM with those of  $(\text{DH}_2)_4\text{H}^+\text{OTf}^-$ , let us note their similarity and differences. Analogous to DES<sup>57</sup> or LTTM,<sup>6</sup>  $(\text{DH}_2)_4\text{H}^+\text{OTf}^-$  has the decreased volatility and increased thermal stability. Similar to DES, it is immiscible with aprotic liquids (e.g.,  $(\text{DH}_2)_4\text{H}^+\text{OTf}^-$  is immiscible with acetonitrile). However,  $(\text{DH}_2)_4\text{H}^+\text{OTf}^-$  does not have a eutectic (the presence of eutectic is a basic property of DES) and that is why should it should be assigned as a LTTM. Nonetheless, thermal decomposition of  $(\text{DH}_2)_4\text{H}^+\text{OTf}^-$  (Fig. 5) indicates that non-protonated  $\text{DH}_2$  molecules are absent in this preparation. In the opposite case, we would observe at least partial decomposition of  $\text{DH}_2$  similar to that depicted in Fig. 2. Besides this, the IR spectrum of  $(\text{DH}_2)_4\text{H}^+\text{OTf}^-$  indicates that not only amino groups but also hydroxyl groups of  $\text{DH}_2$  are protonated. Thermochemical,<sup>58,59</sup>

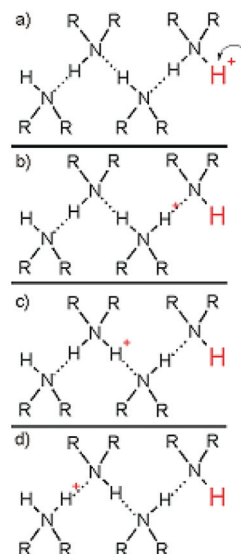


Fig. 7 Scheme of proton charge transfer *via* the soliton mechanism.

acoustic<sup>60</sup> and dielectric<sup>61</sup> studies of mixtures of amines and alcohols demonstrated that H-bonds of  $\text{N}\cdots\text{H}-\text{O}-\text{R}$  type between amine and alcohol molecules are formed in these mixtures.

H-bonds are also formed between the strongly polarized N-H bonds of ammonium ions<sup>62</sup> and the oxygen atoms of hydroxyl groups.<sup>63,64</sup> In  $(\text{DH}_2)_4\text{H}^+\text{OTf}^-$ , containing both ammonium ions and hydroxyl groups, multiple H-bonds exist in the presence of a super acid,<sup>26,39</sup> these H-bonds can join hydroxyl and amine groups of  $\text{DH}_2$  with mobile positive charges (but not protons themselves) *via* the soliton mechanism (Fig. 7). Such a possibility is supported by arguments given in ref. 35 and 65. This mechanism provides mobility of positive charges even for relative immobility of H nuclei over the entire volume of the preparation *via* exchange of  $\sigma$ -bonds and hydrogen bonds:  $\text{O}-\text{H}\cdots\text{N} \leftrightarrow \text{O}\cdots\text{H}-\text{N}$ . Due to this exchange, in  $(\text{DH}_2)_4\text{H}^+\text{OTf}^-$  there is no separation for  $\text{DH}_3^+$  ammonium ions (corresponding with  $\text{H}_2\text{N}^+[(\text{CH}_2)_2\text{OH}]_2$ ) and  $\text{DH}_2$  molecules, necessary for the existence of a eutectic, but a mechanism occurs for mutual transformation of  $\text{DH}_3^+$  ions and  $\text{DH}_2$  molecules.

Thus, the properties of  $(\text{DH}_2)_4\text{H}^+\text{OTf}^-$  are similar to those of LTTM.

Such solvents deserve particular attention as media for electrochemical processes: scrap utilization, electrolysis, electropolishing and separation of metals<sup>66-69</sup> and also in flow accumulators.<sup>7-10</sup>

## Conclusions

The studied copper preparation,  $[\text{Cu}^{2+}\text{DH}_2(\text{DH}^-)][(\text{DH}_2)_4\text{H}^+](\text{OTf}^-)_2$ , is a solution of complex salt  $[\text{Cu}^{2+}\text{DH}_2(\text{DH}^-)]\text{OTf}^-$  in LTTM with composition  $[(\text{DH}_2)_4\text{H}^+]\text{OTf}^-$ . The coordination number of metal atoms in  $[\text{Cu}^{2+}\text{DH}_2(\text{DH}^-)]\text{OTf}^-$  of this solu-

tion does not exceed four, but that in  $\text{Fe}(\text{OTf})_3 \cdot 6\text{DH}_2$  is equal to six (see ESI†); this means that the structural distinction between the two preparations which are similar in composition requires further investigation.

Volatility and decomposition of  $\text{DH}_2$  change noticeably on addition of even small amounts of acid, and this can be rationalized by the soliton mechanism of positive charge transfer over all the volume of  $\text{DH}_2$ , giving rise to integration of all  $\text{DH}_2$  molecules into a collective cation.  $\text{DH}_2$  vaporization also depends on addition of metal salts: addition of iron(III) triflate causes vaporization of  $\text{DH}_2$  remaining after  $\text{DH}_2$  condensation reaction in the range 300–400 °C (see ESI†), however, in the presence of copper(II) triflate  $\text{DH}_2$  does not vaporize but decomposes, although not in the same manner as pure  $\text{DH}_2$  does.

## Acknowledgements

The authors acknowledge Professor Alexander V. Yatsenko from Department of Chemistry, Lomonosov Moscow State University for fruitful discussions and attention to this work. This study was supported by Lomonosov Moscow State University Program of Development.

## References

- 1 A. P. Abbott, G. Capper, D. L. Davies, R. K. Rasheed and V. Tambyrajah, *Chem. Commun.*, 2003, 70–71.
- 2 M. H. Chakrabarti, F. S. Mjalli, I. M. AlNashef, M. A. Hashim, M. A. Hussain, L. Bahadori and C. T. J. Low, *Renewable Sustainable Energy Rev.*, 2014, **30**, 254–270.
- 3 D. V. Wagle, H. Zhao and G. A. Baker, *Acc. Chem. Res.*, 2014, **47**, 2299–2308.
- 4 Q. Zhang, K. De O. Vigier, S. Royer and F. Jérôme, *Chem. Soc. Rev.*, 2012, **41**, 7108–7146.
- 5 E. Durand, J. Lecomte and P. Villeneuve, *Eur. J. Lipid Sci. Technol.*, 2013, **115**, 379–385.
- 6 M. Francisco, A. van den Bruinhorst and M. C. Kroon, *Angew. Chem., Int. Ed.*, 2013, **52**, 3074–3085.
- 7 T. M. Anderson, D. Ingersoll, A. J. Rose, C. L. Staiger and J. C. Leonard, *Dalton Trans.*, 2010, **39**, 8609–8612.
- 8 H. D. Pratt III, A. J. Rose, C. L. Staiger, D. Ingersoll and T. M. Anderson, *Dalton Trans.*, 2011, **40**, 11396–11401.
- 9 H. D. Pratt III, J. C. Leonard, L. A. M. Steele, C. L. Staiger and T. M. Anderson, *Inorg. Chim. Acta*, 2013, **396**, 78–83.
- 10 H. D. Pratt III, D. Ingersoll, N. S. Hudak, B. B. McKenzie and T. M. Anderson, *J. Electroanal. Chem.*, 2013, **704**, 153–158.
- 11 Y. Yoshida, H. Tanaka, G. Saito, L. Ouahab, H. Yoshida and N. Sato, *Inorg. Chem.*, 2009, **48**, 9989–9991.
- 12 S. Hayashi and H.-O. Hamaguchi, *Chem. Lett.*, 2004, **33**, 1590–1591.
- 13 Y. Yoshida and G. Saito, *J. Mater. Chem.*, 2006, **16**, 1254–1262.
- 14 R. E. Del Sesto, T. M. McCleskey, A. K. Burrell, G. A. Baker, J. D. Thompson, B. L. Scott, J. S. Wilkes and P. Williams, *Chem. Commun.*, 2008, 447–449.
- 15 A. P. Abbott and K. J. McKenzie, *Phys. Chem. Chem. Phys.*, 2006, **8**, 4265–4279.
- 16 N. R. Brooks, S. Schaltin, K. Van Hecke, L. Van Meervelt, J. Fransaer and K. Binnemans, *Dalton Trans.*, 2012, **41**, 6902–6905.
- 17 S. Schaltin, N. R. Brooks, L. Stappers, K. Van Hecke, L. Van Meervelt and K. Binnemans, *Phys. Chem. Chem. Phys.*, 2012, **14**, 1706–1715.
- 18 P. Hapiot and C. Lagrost, *Chem. Rev.*, 2008, **108**, 2238–2264.
- 19 S. Schaltin, N. R. Brooks, K. Binnemans and J. Fransaer, *J. Electrochem. Soc.*, 2011, **158**, D21–D27.
- 20 N. R. Brooks, S. Schaltin, K. Van Hecke, L. Van Meervelt, K. Binnemans and J. Fransaer, *Chem.–Eur. J.*, 2011, **17**, 5054–5059.
- 21 C. W. Davies and B. N. Patel, *J. Chem. Soc. A*, 1968, 1824–1828.
- 22 R. Tauler, E. Casassas and B. M. Rode, *Inorg. Chim. Acta*, 1986, **114**, 203–209.
- 23 A. Karadag, V. T. Yilmaz and C. Thoene, *Polyhedron*, 2001, **20**, 635–641.
- 24 J. Madarasz, P. Bombicz, M. Czugler and G. Pokol, *Polyhedron*, 2000, **19**, 457–463.
- 25 K. Majid, R. Mushtaq and S. Ahmad, *E-J. Chem.*, 2008, **5**(s1), S969–979.
- 26 C. A. Reed, *Acc. Chem. Res.*, 2013, **46**, 2567–2575.
- 27 P. Dwards, G. Wilkinson, K. M. A. Malik and M. B. Hursthouse, *J. Chem. Soc., Chem. Commun.*, 1979, 1158–1159.
- 28 P. G. Edwards, G. Wilkinson, M. B. Hursthouse and K. M. A. Malik, *J. Chem. Soc., Dalton Trans.*, 1980, 2467–2475.
- 29 M. Shahid, A. Siddique, I. A. Ansari, F. Sama, S. Chibber, M. Khalid, Z. A. Siddiqi and Md. S. H. Faizi, *J. Coord. Chem.*, 2015, **68**, 848–862.
- 30 J.-N. Feng, Y.-Z. Zhou, H.-J. Zhu and S.-J. Tu, *Z. Kristallogr. - New Cryst. Struct.*, 2006, **221**, 343–344.
- 31 J. Blaszczyk, Z. Lu, Y. Li, H. Yan and X. Ji, *Cell & Bioscience*, 2014, **4**, 52–13.
- 32 M. Meepriruk and K. J. Haller, *Acta Crystallogr., Sect. C: Cryst. Struct. Commun.*, 2013, **69**, 1077–1080.
- 33 G. E. López, I. Colón-Díaz, A. Cruz, S. Ghosh, S. B. Nicholls, U. Viswanathan, J. A. Hardy and S. M. Auerbach, *J. Phys. Chem. A*, 2012, **116**, 1283–1288.
- 34 U. Viswanathan, D. Basak, D. Venkataraman, J. T. Fermann and S. M. Auerbach, *J. Phys. Chem. A*, 2011, **115**, 5423–5434.
- 35 V. Zoete and M. Meuwly, *J. Chem. Phys.*, 2004, **120**, 7085–7094.
- 36 H. J. Berthold, E. Vonholdt, R. Wartchow and T. Vogt, *Z. Kristallogr.*, 1992, **200**, 225–235.
- 37 I. Olovsson, *Acta Chem. Scand.*, 1960, **14**, 1466–1474.
- 38 M. V. Vener and N. B. Librovich, *Int. Rev. Phys. Chem.*, 2009, **28**, 407–434.
- 39 C. Knight and G. A. Voth, *Acc. Chem. Res.*, 2012, **45**, 101–109.
- 40 B. Chan, J. E. Del Bene and L. Radom, *J. Am. Chem. Soc.*, 2007, **129**, 12197–12199.

- 41 T. Fujinaga and I. Sakamoto, *J. Electroanal. Chem.*, 1976, **73**, 235–246.
- 42 S. Ichikawa, I. Tomita, A. Hosaka and T. Sato, *Bull. Chem. Soc. Jpn.*, 1988, **61**, 513–520.
- 43 G. V. Fetisov, in *Synchrotron radiation. Structure research techniques of materials*, ed. L. A. Aslanov, FIZMATLIT, Moscow, 2007, ch. 5, pp. 488–579. ISBN 978-5-9221-0805-8 [In Russian].
- 44 G. Bunker, *Introduction to XAFS: A practical guide to X-ray Absorption Fine Structure*, Cambridge University Press, 2010, p. 260.
- 45 A. A. Chernyshov, A. A. Veligzhanin and Y. V. Zubavichus, *Nucl. Instrum. Methods Phys. Res., Sect. A*, 2009, **603**, 95–98.
- 46 M. Newville, *J. Synchrotron Radiat.*, 2001, **8**, 322–324.
- 47 B. Ravel and M. Newville, *J. Synchrotron Radiat.*, 2005, **12**, 537–541.
- 48 J. J. Rehr, *Radiat. Phys. Chem.*, 2006, **75**, 1547–1558.
- 49 J. J. Rehr and R. C. Albers, *Phys. Rev. B: Condens. Matter*, 1990, **41**, 8139–8149.
- 50 J. J. Rehr and R. C. Albers, *Rev. Mod. Phys.*, 2000, **72**, 621–654.
- 51 L. Campbell, L. Hedin, J. J. Rehr and W. Bardtszewski, *Phys. Rev. B: Condens. Matter*, 2002, **65**, 064107.
- 52 J. J. Rehr and A. L. Ankudinov, *Radiat. Phys. Chem.*, 2004, **70**, 453–463.
- 53 J. J. Rehr and A. L. Ankudinov, *Coord. Chem. Rev.*, 2005, **249**, 131–140.
- 54 D. Lee, L. Sorace, A. Caneschi and S. J. Lippard, *Inorg. Chem.*, 2001, **40**, 6774–6774.
- 55 M. L. Kennard and A. Allelsen, *Ind. Eng. Chem. Fundam.*, 1985, **24**, 129–140.
- 56 R. I. Khusnutdinov, A. R. Bayguzina, L. I. Gimaletdinova and U. M. Dzhemilev, *Russ. J. Org. Chem.*, 2012, **48**, 1191–1196. © Pleiades Publishing, Ltd., 2012.
- 57 E. Durand, J. Lecomte and P. Villeneuve, *Eur. J. Lipid Sci. Technol.*, 2013, **115**, 379–385.
- 58 J. Fernandez, M. I. Paz Andrade, M. Pintos, F. Sarmiento and R. Bravo, *J. Chem. Thermodyn.*, 1983, **15**, 581–584.
- 59 M. K. Duttachoudhury and H. B. Mathur, *J. Chem. Eng. Data*, 1974, **19**, 145–147.
- 60 A. C. H. Chandrasekhar and A. Krishnaiah, *Phys. Chem. Liq.*, 1988, **17**, 315–321.
- 61 G. M. Kalamse, P. G. Gawali and R. Pande, *Int. J. Chem. Sci.*, 2004, **2**, 426–432.
- 62 P. A. Hunt, C. R. Ashworth and R. P. Matthews, Hydrogen bonding in ionic liquids, *Chem. Soc. Rev.*, 2015, **44**, 1257–1288.
- 63 S. V. Bogatkov, V. N. Romashov, N. I. Kholdyakov and E. M. Cherkasova, *Zh. Obshch. Khim.*, 1969, **39**, 266–268.
- 64 A. P. Ligon, *J. Phys. Chem. A*, 2000, **104**, 8739–8743.
- 65 X. F. Pang, *Prog. Biophys. Mol. Biol.*, 2013, **112**, 1–32.
- 66 A. P. Abbott, G. Capper, K. J. McKenzie and K. S. Ryder, *J. Electroanal. Chem.*, 2007, **599**, 288–294.
- 67 A. P. Abbott, K. El Ttaib, G. Frisch, K. J. McKenzie and K. S. Ryder, *Phys. Chem. Chem. Phys.*, 2009, **11**, 4269–4277.
- 68 A. M. Popescu, V. Constantin, A. Cojocaru and M. Olteanu, *Rev. Chim.*, 2011, **62**, 206–211.
- 69 E. Gómez, P. Cojocaru, L. Magagnin and E. Valles, *J. Electroanal. Chem.*, 2011, **658**, 18–24.